ACS APPLIED NANO MATERIALS

www.acsanm.org Article

Optically Activatable Double-Drug-Loaded Perfluorocarbon Nanodroplets for On-Demand Image-Guided Drug Delivery

Catalina-Paula Spatarelu, Austin Van Namen, and Geoffrey P. Luke*

Cite This: https://doi.org/10.1021/acsanm.1c01303 Read Online

ACCESS | Metrics & More | Article Recommendations | Supporting Information

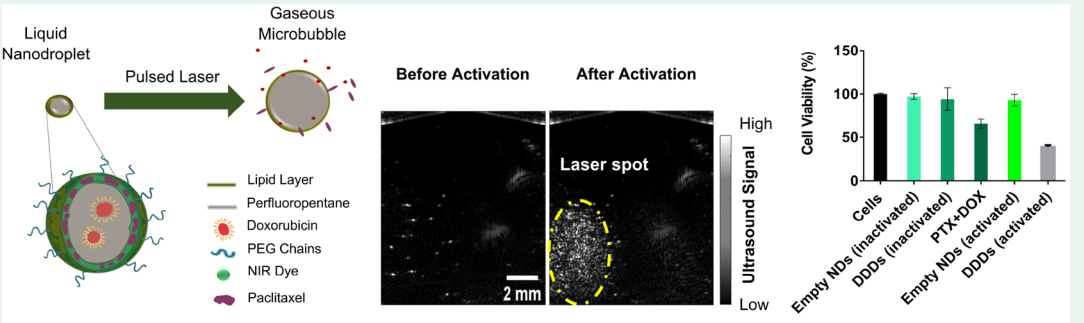

ABSTRACT: Phase-changing nanodroplets have been studied as externally activatable in situ microbubble precursors. The nanodroplets can be triggered to vaporize with an external optical or acoustic energy source, and the resulting microbubbles can be visualized with high sensitivity using ultrasound imaging. Because of their nanoscale size, this type of construct is attractive for the encapsulation and on-site, on-demand release of therapeutics. Here, we develop a double-drug loaded nanodroplet platform that can coencapsulate paclitaxel and doxorubicin, and release them upon external laser activation. Nanodroplets are characterized in terms of size, stability, protein interaction, and drug release. Their capacity to concurrently release the two drugs and generate ultrasound contrast is demonstrated in vitro. The efficacy of dual-drug loaded nanodroplets is compared in vitro with that of free drug formulations, and potential mechanisms of their enhanced cytotoxic behavior are explored. Overall, the results show that the nanodroplets are a versatile platform for on-demand image-guided drug delivery.

KEYWORDS: *phase-changing nanodroplets, ultrasound theranostics, image-guided cancer therapy, drug-delivery, combination therapy*

1. INTRODUCTION

Effective cancer therapy must achieve a localized effect on the diseased tissues while minimizing systemic toxicity.[1] Taking into account years of research and development into the field of nanomedicine, it has become clearer that no single formulation can achieve this feat. Rather, a synergy of techniques, including but not limited to stratification of patients and tumors, and personalized treatment plans is a promising way forward. In this context, the field of image-guided drug delivery emerged as a way of bringing the strengths of imaging to optimize drug therapy,[2] either by allowing the visualization of on-site accumulation, the monitoring of on-target and off-target distribution of carriers, or the quantification of drug release.[3] Each of these functions, and more, could be employed to gain valuable information for treatment planning, patient stratification, and therapy response monitoring.[1]

As an image-guided drug delivery modality, ultrasound has a series of advantages that make it preferable over other physical modalities such as magnetic resonance imaging or positron emission tomography. It is cost-effective and generally accessible, while simultaneously being a safe, nonionizing imaging technique. Ultrasound imaging provides real-time imaging several centimeters deep in soft tissue with submillimeter resolution. Diagnostic ultrasound imaging with contrast agents, such as microbubbles, relies on the acoustic impedance mismatch between the water-based tissue background and gaseous microbubbles to create high-contrast images.[4] This status has made microbubbles attractive to drug and gene delivery applications as well, particularly for image-guided strategies.[5]

However, despite their FDA-approved status, in the context of image-guided drug delivery microbubbles have certain disadvantages that limit their use.[6] Because of their size, they are confined in the vasculature and not able to extravasate into the tumor tissue.[7] Additionally, the loading of drugs in

Received: May 17, 2021
Accepted: August 5, 2021

therapeutically relevant quantities remains a challenge.[5] Finally, for drug-loaded microbubbles, the release of the drugs is correlated to the disappearance of the ultrasound contrast, which makes it difficult to trace the drugs after sonication. To address these shortcomings, nanoconstructs that can be transformed into microbubbles in vivo by external stimuli were proposed as an alternative.[8]

Emulsions have long been used in the clinic as drug carriers, and nanoemulsions of several types have been proposed as passive drug-delivery systems.[9,10] Among them, perfluorocarbon nanoparticles (NPs) are a multifunctional theranostic technology that have been tested in preclinical models of cancer,[8,10] atherosclerosis,[11] and tissue ablation.[12] These particles consist of a Perfluorocarbon (PFC) core stabilized by a surfactant, polymer or lipid layer, and dispersed in an aqueous media. Perfluorocarbons such as perfluoropentane (PFP), perfluorooctyl bromide (PFOB), or perfluoro-15-crown-5-ether (PFCE) have been studied in this context and make up the active ingredient of FDA-approved contrast agents. Perfluorocarbon nanodroplets benefit from being biocompatible at large doses,[13] with no observed toxicity or carcinogenicity,[13,14] and a biological half-life that can range from minutes, in the case of PFP emulsions[15] up to days in the case of PFCE[16] and PFOB.[17] The half-life of perfluorocarbon nanoparticles has been shown to depend on the properties of the core,[18−20] such as boiling point, solubility in water,[20] molecular weight, the nature of the stabilizing shell,[16] and the size of particles.[21] PFC nanodroplets are kept stable by the Laplace pressure experienced inside the nanodroplets, that increases the boiling point of the core,[22,23] which is necessary for PFCs with boiling points lower than physiological temperature, like PFP that boils at 29 °C. As their name suggests, PFC nanodroplets are nanosized, hence they can address two of the main issues with the microbubbles system: they have the potential to extravasate into the tumor tissue through the endothelial gaps, and have considerably longer circulation times due to their small size and increased stability.[23]

Compared to microbubbles, nanodroplets are not highly echogenic, as they lack the mismatch in acoustic impedance. When exposed to the proper acoustic, optical, or magnetic stimulus, however, the core undergoes a phase transition, resulting in gaseous microbubbles that can then be clearly visualized in ultrasound images.[10] For optically activated nanodroplets, such as the ones described in this study, the stimulus for activation is optical energy in the form of short-pulsed laser light. The light is absorbed by the encapsulated chromophore(s) and converted into thermal energy, resulting in a localized temporary temperature increase and broadband pressure waves. When the laser is above a threshold fluence, the perfluorocarbon receives enough energy to transition from liquid to gas, a phenomenon that is called optical droplet vaporization.[24]

In addition to their size advantage over microbubbles, the drug loading capabilities of single-drug perfluorocarbon nanodroplet formulations have been previously investigated,[25] demonstrating sufficient encapsulation efficiency for in vivo efficacy.[26,27] However, due to the complexity of tumors, single drug strategies might not be always effective; combination chemotherapy is accepted as increasingly important for improved long-term outcomes.[28] Unlike monotherapy, using two or more chemotherapeutics simultaneously can maximize therapeutic efficacy and overcome drug resistance of certain cancer cell subpopulations.[29] The main motivation for combination therapy is in the possibility of using drugs with distinct mechanisms of actions and pathways, that act on different elements on the cell and potentially at different cell cycle stages.[30] Synergies between the drugs used can lead to better outcomes,[31,32] doxorubicin and paclitaxel being a prime example of ratio-dependent synergistic effects.[33] However, maintaining a constant ratio of drugs that reaches the tumor site is a challenge,[31] since each drug has a different pharmacokinetic profile, especially in the case of drugs that have drastically different solubilities in aqueous media.[32] Combining both therapeutic molecules in one platform is beneficial for controlling their pharmacokinetic profiles, and to ensure that the ratio between the amounts of the two drugs reaching the tumor site is the same as the one administered. Thus, adding multidrug loading capabilities to perfluorocarbon nanodroplets is needed in order to expand their clinical potential.

Our work aims to address this need by developing a platform technology based on perfluorocarbon nanodroplets that can be employed for combination therapy. Unlike previous studies that look at the efficiency of single-drug-loaded droplets,[34] our work herein describes a way to achieve on-demand simultaneous delivery of two compounds with different hydrophilicities and a method to quantify the concentration-dependent ultrasound magnitude obtained after drug release.

In this study, we describe a new double-drug loaded perfluorocarbon nanodroplet platform, capable of encapsulating both hydrophilic and hydrophobic therapeutics. Doxorubicin and paclitaxel are used as the model drugs in our study due to their common employment in combination therapy for a variety of cancers.[35,36] The nanodroplets are also loaded with a near-infrared (NIR) absorbing dye to enable external optical activation. The release of paclitaxel and doxorubicin from the nanodroplets upon exposure to a pulsed NIR laser stimulus is studied in vitro. In addition, the ultrasound image contrast is evaluated for nanodroplets before and after activation, correlating the total signal increase with the concentration of nanodroplets being triggered. Finally, this study investigates the effect of time of incubation before activation on cell viability, and explores more complex formulations for multiplexed nanodroplets. Our study establishes perfluorocarbon nanodroplets as a viable platform for coencapsulation and image-guided release of both hydrophobic and hydrophilic drugs.

2. EXPERIMENTAL SECTION

Synthesis of Dual-Drug Nanodroplets. The dual-drug loaded nanodroplets (DDDs) were synthesized by a double emulsion method. The first emulsion was synthesized by a thin-layer hydration−sonication method. Typically, a mixture of dipalmitoylphosphatidylcholine (DPPC, NOF America), 1,2-distearoyl-*sn*-glycero-3-phosphoethanolamine-*N*-[amino(polyethylene glycol)-2000] (DSPE-PEG_{2000}, NOF America) and cholesterol (Alfa Aesar), in a molar ratio of 35:15:50 was added to 3 mL of chloroform and evaporated under vacuum (250 mbar) with a rotary evaporator at 38.5 °C. Paclitaxel (2 mg, Fisher Scientific) was dissolved together with the lipids in chloroform for coassembly. To enable laser activation capabilities of the nanodroplets, a NIR dye, Epolight 3072 (Epolin) with a maximum absorbance at 1064 nm was added together with the lipid mixture in chloroform. After the mixture evaporated and formed a thin film, 3 mL of 2:3 v/v water:Dulbecco's phosphate-buffered saline (Corning) was used for rehydration, and the mixture was subjected to a sonicating bath for 5 min at room temperature. Next,

https://doi.org/10.1021/acsanm.1c01303
ACS Appl. Nano Mater. XXXX, XXX, XXX−XXX

the mixture was dispersed with a sonication probe (QSonica, Q700, 1/8 in. microtip) for 30 s, at 27 W/cm^2 in an ice-bath to prevent the sample from overheating.

The second emulsion was constituted by aqueous doxorubicin solution (Advanced ChemBlocks) in perfluoropentane (PFP, Fluoromed). The doxorubicin solution (0.25 mL, 7.0 mg/mL) was added to a mixture of PFP (1.5 mL) and emulsifier (Krytox FSL, 20 μL), and sonicated with the ultrasonic probe under the same conditions as previously described. Different formulations were tested before settling for these specific ratios between the drug solution, PFP, and emulsifier. A volume of 200 μL of this emulsion was added to the lipid-paclitaxel mixture and sonicated for an additional 30 s. For empty nanodroplets, this step consisted of only adding the PFP, followed by the same sonication regimen.

The nanodroplet mixture was centrifuged at 43 rcf, to remove large aggregates and unencapsulated components, such as paclitaxel or Epolight, that settle out of the dispersion due to poor solubility in water. This was followed by collection of the supernatant and two more steps of centrifugation at 2100 rcf. For each of these steps, the supernatant was discarded and replaced with distilled water, to remove micelles or unincorporated doxorubicin.

Extrusion of DDDs. After synthesis and washing steps, the DDDs were downsized by extrusion through a mini-extruder (Avanti Lipids) with a 0.4 μm polycarbonate membrane for a total of five passes. The process was undertaken at room temperature, using a volume of 1 mL per batch. For cell studies, the sample was filtered through a sterilizing 0.2 μm syringe filter (Whatman Puradisc, poly(ether sulfone)) to ensure sterility.

Size Characterization. Average nanodroplet diameter and size distribution were determined by a Malvern Zetasizer Dynamic Light Scattering (DLS) instrument after 100× dilution to ensure the concentration was low enough for single-scattering events. All samples were subjected to three measurements each, with an automatic number of runs per measurement, as determined by the instrument. Size is reported as the d-average, together with the standard deviation of the three measurements. The stability of the nanodroplets that were kept at 4 °C was estimated by the evolution of size in time, as reported by DLS.

Drug Loading Measurement. The nanodroplets were dissolved in a 50/50 v/v mixture of acetonitrile and water and heated in a water bath to 60 °C for 1 h to ensure the destruction of all nanodroplets. The paclitaxel concentration was determined by UV−Vis (Varian Cary 50) absorption at 229 nm, by means of a previously constructed calibration curve. The absorbance of empty nanodroplets was recorded to account for any effects from the matrix components, and the value of absorption at 229 nm was corrected by that registered in the empty nanodroplets spectra. For the determination of doxorubicin content in the dual drug nanodroplets, the nanodroplets were dissolved as described here and measured with a spectrofluorometer (HORIBA Fluoromax) using a 480 nm/590 nm excitation/emission against a calibration curve.

The encapsulation efficiency, ee, was determined by the formula:

$$\text{ee, \%} = \frac{\text{mass of drug measured, mg}}{\text{mass of drug added initially, mg}} 100$$

The approximate $\text{mass}_{\text{drug}}/\text{mass}_{\text{particle}}$ for each of the two drugs was computed by dividing the mass of drug encapsulated measured as described above, over the approximate mass of a particle. The mass of a particle was estimated using the total mass of components/number of particles in the sample, correcting by the losses during wash steps that were accounted with by the DLS concentration measurement before and after the washing steps.

Drug-Release Study. Nanodroplets were diluted 20× in phosphate-buffered saline (PBS), and samples were incubated in a water bath at 37 °C under gentle mixing to combat any sedimentation. Samples were taken at the beginning of the study, after 0.5 h and after 1 h. At the 30 min time point, the corresponding samples (noted as "laser-activated") were activated by 1064 nm pulsed laser (Opotek Phocus HE) with a fluence of 15 mJ/cm^2, for a total of 5 s at 10 Hz pulse repetition frequency. The samples were centrifuged and the supernatant was measured for the amount of drug based on the methods described above. The pellet was similarly collected to measure the drug left in the droplets. The amount of unencapsulated drug measured at the initial time point was subtracted from the following measurements. For each of the measurements, the same batch of nanodroplets was divided in two parts—one that was not activated to serve as a control, and one that was exposed to the laser at the 30 min time point. For doxorubicin measurements, the samples collected from the inactivated nanodroplets were exposed to laser illumination equivalent to the activated nanodroplets to account for photobleaching effects.

Drug-Release in the Presence of Protein Corona. To study the influence of hard protein corona on the release of drugs of nonactivated compared to activated nanodroplets, three different media were used: distilled water, 10% fetal bovine serum (FBS) solution, and 100% FBS. Nanodroplets were incubated in the respective media for 1 h, at 37 °C, under gentle stirring, followed by washing and replacement of their suspension media with PBS. After 10 min in a water bath at 37 °C, nanodroplets from the "activated" group were illuminated with the pulsed NIR laser. Control samples followed the same procedure, except for the activation step. The samples were centrifuged, and the released doxorubicin was measured in the supernatant.

Ultrasound Imaging. Polyacrylamide gel phantoms were obtained as previously described.[37] Briefly, a 10% polyacrylamide gel was prepared from a solution of acrylamide:bis(acrylamide) (29:1) adding up to 1.5% v/v nanodroplets suspension, and *N,N,N′,N′*-tetramethylethylendiamine (TEMED) and ammonium peroxodisulfate (APS) as initiator system. Each phantom was set on an in-house built platform and imaged with a L22−8v Verasonics linear array ultrasound transducer connected to a Verasonics Vantage 256 imaging system. Images were acquired using plane-wave acquisition with five compounding angles (−18, −9, 0, 9, 18 degrees) before and after the laser pulse(s). Results are presented as the difference between the average signal after the trigger and the previous signal, as well as the signal magnitude in the region of interest of the scan.

To investigate the correlation between the concentration of nanodroplets in the phantom and the change in signal magnitude recorded by ultrasound, a series of phantoms with various volumetric percentages of nanodroplets dispersion were created: 0.1%, 0.25%, 0.5%, 1%, 1.5%. The concentration, expressed as particles/mL, was determined from the DLS results using the Malvern Zetasizer's built-in concentration measurement tool. To avoid any mismatch, the same sample of nanodroplets was used for the whole series, and four spots on each phantom were averaged to account for any heterogeneity for each of the studied concentrations. A 6 mm × 3.25 mm rectangular ROI was selected for each of the spots on the phantoms, with the signal being computed as the difference between the average sum of pixel values in the ROI after activation and the average sum of pixel values in the ROI prior to activation.

In Vitro Cell Toxicity Studies. FaDu cells were used to assess the cytotoxicity of drug-loaded nanodroplets. Cells were passaged and seeded into 24-well plates in Dulbecco's Modified Eagle Medium with 10% FBS, and 1% mixture of penicillin/streptomycin at a 0.04 × 10^6 cell density. The cells were left to attach and grow overnight in an incubator at 37 °C and 5% CO_2 concentration, then subjected to various formulations. The studied groups were nontreated cells for control, inactivated empty nanodroplets, inactivated DDDs, free paclitaxel + doxorubicin, laser-activated empty nanodroplets, and laser-activated DDDs. Nanodroplets were added to a 250× dilution in the total volume of each well, or around 4.56 × 10^7 nanodroplets/well. The concentration of loaded paclitaxel was 1.7 μM and that of loaded doxorubicin was 0.28 μM with respect to the well volume in the wells that were subjected to drug-loaded nanodroplets. For the free drug formulation, the same concentrations of both paclitaxel and doxorubicin were used. The working volume throughout the study was kept constant at 1 mL in each well. Each group was triplicated. After adding the corresponding formulation, the cells were allowed to

https://doi.org/10.1021/acsanm.1c01303
ACS Appl. Nano Mater. XXXX, XXX, XXX−XXX

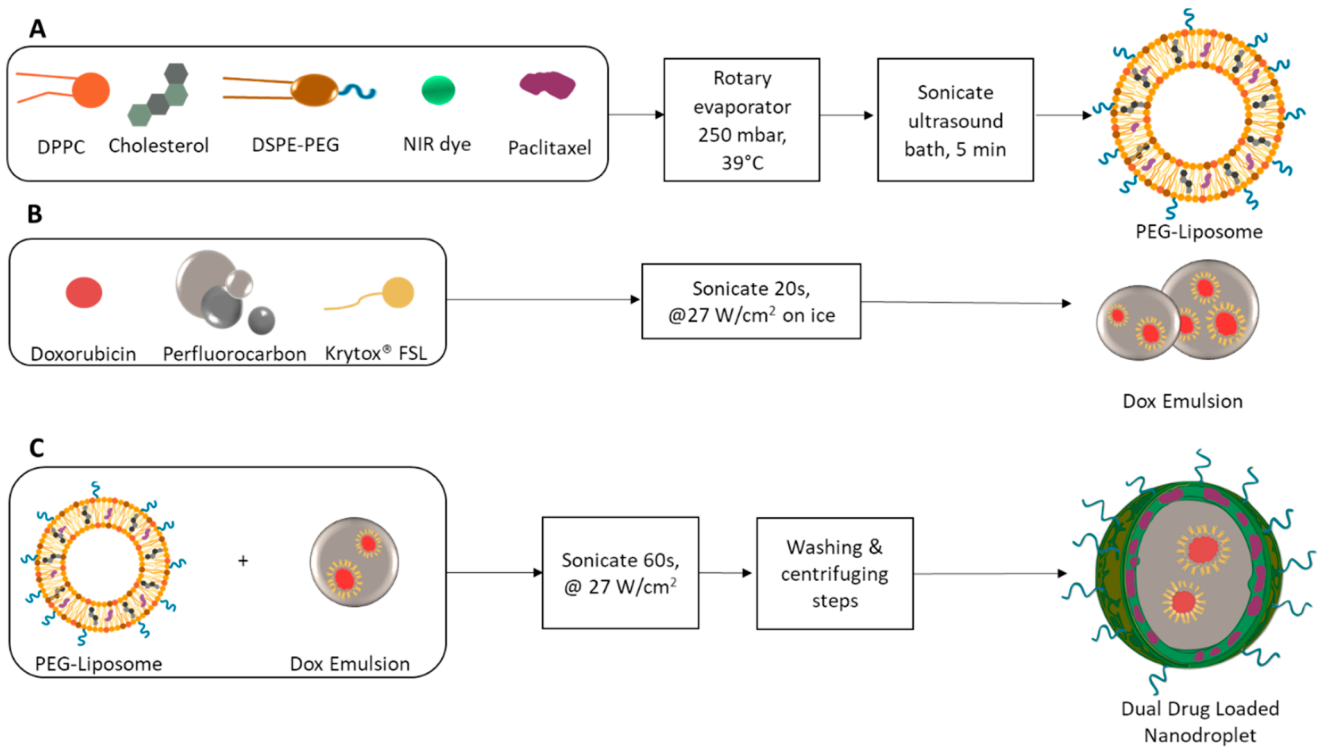

Figure 1. Nanodroplets fabrication steps: (A) liposome formation by thin-film formation and rehydration; (B) core emulsion formation by sonication; (C) combining the two emulsions under sonication to form the double-emulsion construct.

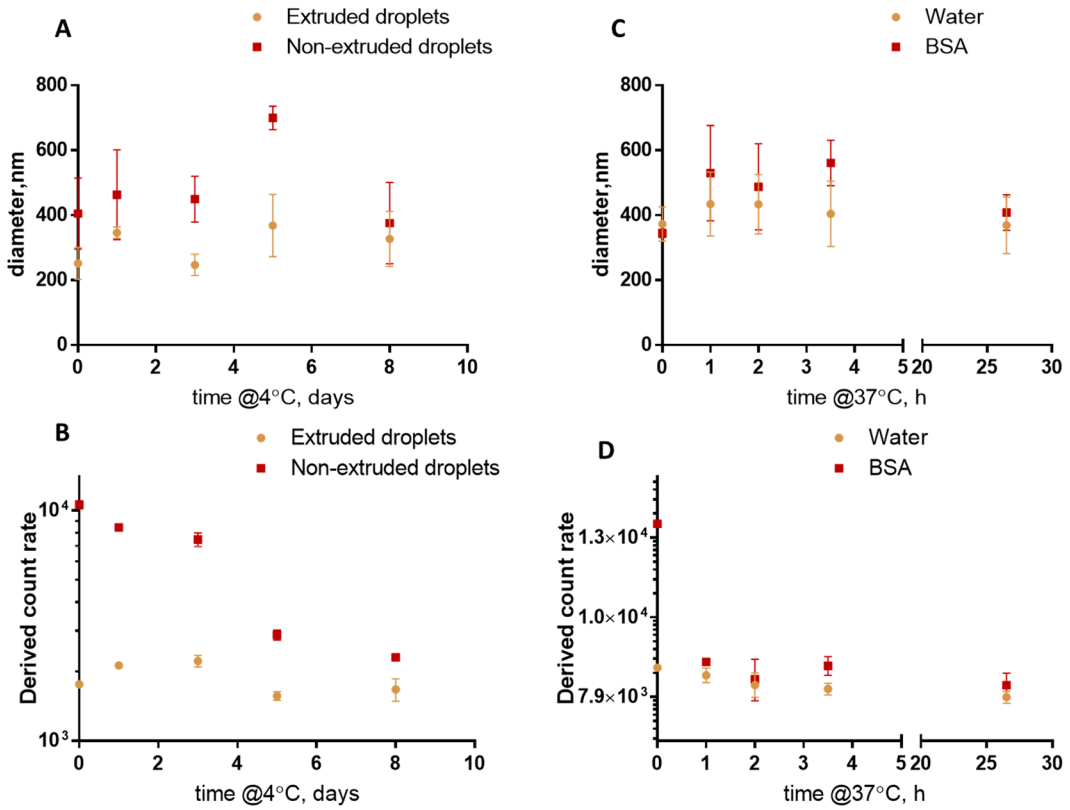

Figure 2. (A) Size change of extruded vs nonextruded nanodroplets stored at 4 °C as a water dispersion; (B) derived count rate change of extruded compared to nonextruded nanodroplets stored at 4 °C; (C) size evolution of nanodroplets incubated at 37 °C in water and bovine serum albumin solution; (D) derived count rate change of nanodroplets incubated at 37 °C in water and bovine serum albumin solution—40 mg/mL. Error bars show the standard deviation obtained from triplicate measurements.

https://doi.org/10.1021/acsanm.1c01303
ACS Appl. Nano Mater. XXXX, XXX, XXX−XXX

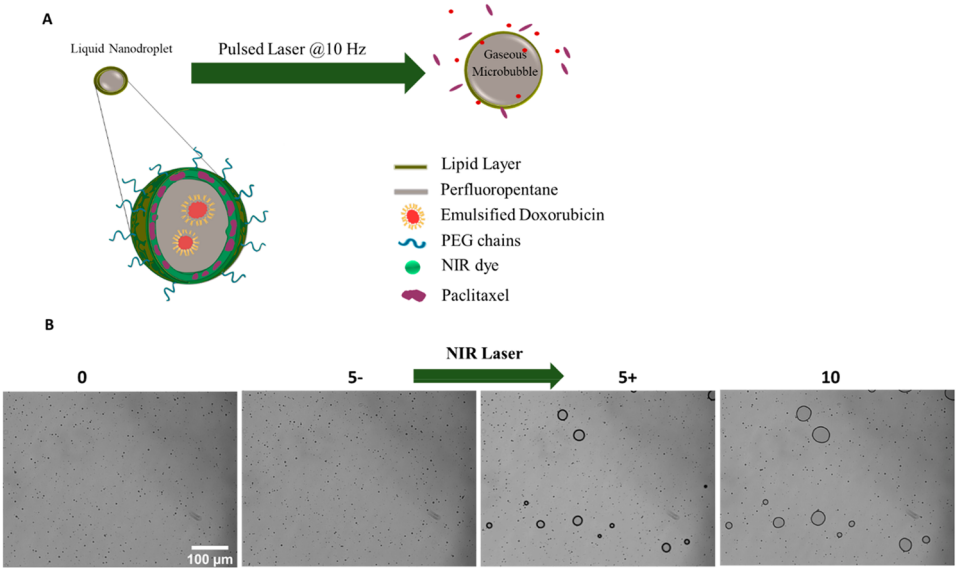

Figure 3. (A) Schematic of dual-drug loaded nanodroplets and their activation under the action of pulsed laser; (B) brightfield image of droplets prior to activation (0), 5 min after the initial time point (5-), immediately after activation (5+), and 5 min after the moment of activation (10).

rest for 10 min in the incubator, followed by the subsequent activation (by laser) of the specified groups in vitro. The cells were then incubated for 4 h, followed by washing with PBS and a (3-(4,5-dimethylthiazol-2-yl)-2,5-diphenyltetrazolium bromide) (MTT) assay to assess cell viability.

Cell Sonoporation Experiment. To probe the effect of mechanical events occurring during the phase transition of nanodroplets, such as cell sonoporation, FaDu cells were subjected to the same doxorubicin concentration (0.2 ug/mL) either as a free drug, together with empty nanodroplets, or formulated in a nanodroplet. Each formulation was analyzed in the case of laser-activated samples or inactivated samples. The same protocol to the cell toxicity study was followed to evaluate the cell viability of the different groups.

In Vitro Time of Incubation Influence. The influence of exposure time of cells to loaded nanodroplets was studied by incubating FaDu cells with loaded nanodroplets for 10 min, 30 min, and 1 h, followed by the replacement of the media and activation of the internalized/bound nanodroplets, and an MTT assay to assess the effects on cell viability. For each of the time points, the study included control wells that were subjected to the same incubation regimen but not activated with the laser. All samples and controls were performed in triplicate.

Internalization of Nanodroplets Study. FaDu cells were plated at a density of 0.5×10^4 cells/mL on a MatTek 35 mm, collagen-coated 14 mm diameter glass well and left to attach overnight. Cells were incubated with FITC-labeled empty nanodroplets, obtained by the procedure described before by replacing 10% of the weight of DSPE-PEG with a FITC-DSPE PEG (Nanocs). Two samples were included, one in which cells were incubated with nanodroplets for 10 min, and another in which the incubation time was 1 h. The final dilution of nanodroplets in both samples was 100× compared to the stock solution of nanodroplets, and the same batch was used for both samples. After incubation, the media was aspirated, and cell layer washed with fresh PBS 3 times. A 300 mM solution of 4′,6-diamidino-2-phenylindole (DAPI, Thermofisher) was used to stain the nuclei as described in the supplier's protocol.[38] Next, a Cell Mask Deep-red membrane stain (Thermofisher) was used to stain the cell plasma membrane following the supplier's protocol.[39] The staining steps were followed by washing steps and a final cell fixation procedure with formaldehyde 3.5% w/v. Confocal images were acquired right after cell fixation, with a ZEISS LSM 800 laser point scanning confocal microscope with Airyscan enhanced resolution, at a magnification of 20×.

3. RESULTS AND DISCUSSION

Nanodroplets Synthesis and Characterization. Figure 1 shows a schematic of the steps involved in the synthesis of DDDs. First, a NIR-dye, paclitaxel containing liposome is created. Second, the core emulsion of doxorubicin suspended in perfluoropentane is synthesized. Finally, the preformed liposomes are combined with the emulsified doxorubicin to create phase-changing, double-drug loaded nanodroplets. The synthesis steps shown in the schematic are followed by a series of centrifugation and washing steps, and finally, an extrusion process for sizing.

The average hydrodynamic diameters of the nanodroplets as measured by dynamic light scattering were 195.70 ± 27.38 nm and 337.40 ± 50.07 nm diameter for extruded nanodroplets, and nonextruded nanodroplets, respectively, immediately following the synthesis and washing steps (Figure 2A).

Size was also used as an indicator of nanodroplets' stability, with coalescence and aggregation leading to larger sizes. Dual-drug loaded nanodroplets were dispersed in distilled water, stored in the refrigerator at 4 °C, and measured periodically over the course of 8 days (Figure 2A). Nanodroplets stored in this manner showed good stability over the time of the experiment, with size slightly increasing in the case of both extruded and nonextruded nanodroplets. On the other hand, the derived count rate of the two samples shows more of a pronounced difference in evolution. In the case of extruded nanodroplets, the derived count rate showed a 5% decrease between the day 0 and day 8 time points (Figure 2B), while the nonextruded sample decreased by 78% compared to the initial time point. These measurements highlight the need for the sizing procedure, especially when longer-term storage is considered. The intensity-weighed distribution of nanodroplets (Supplementary Figure 1) from both samples showed a widening of the peaks, as well as the appearance of smaller peaks, and larger peaks which might indicate a disproportionation process such as Ostwald ripening happening.

To simulate the conditions nanodroplets would be subjected to during circulation, extruded nanodroplets were incubated with a 40 mg/mL bovine serum albumin solution at 37 °C,

https://doi.org/10.1021/acsanm.1c01303
ACS Appl. Nano Mater. XXXX, XXX, XXX−XXX

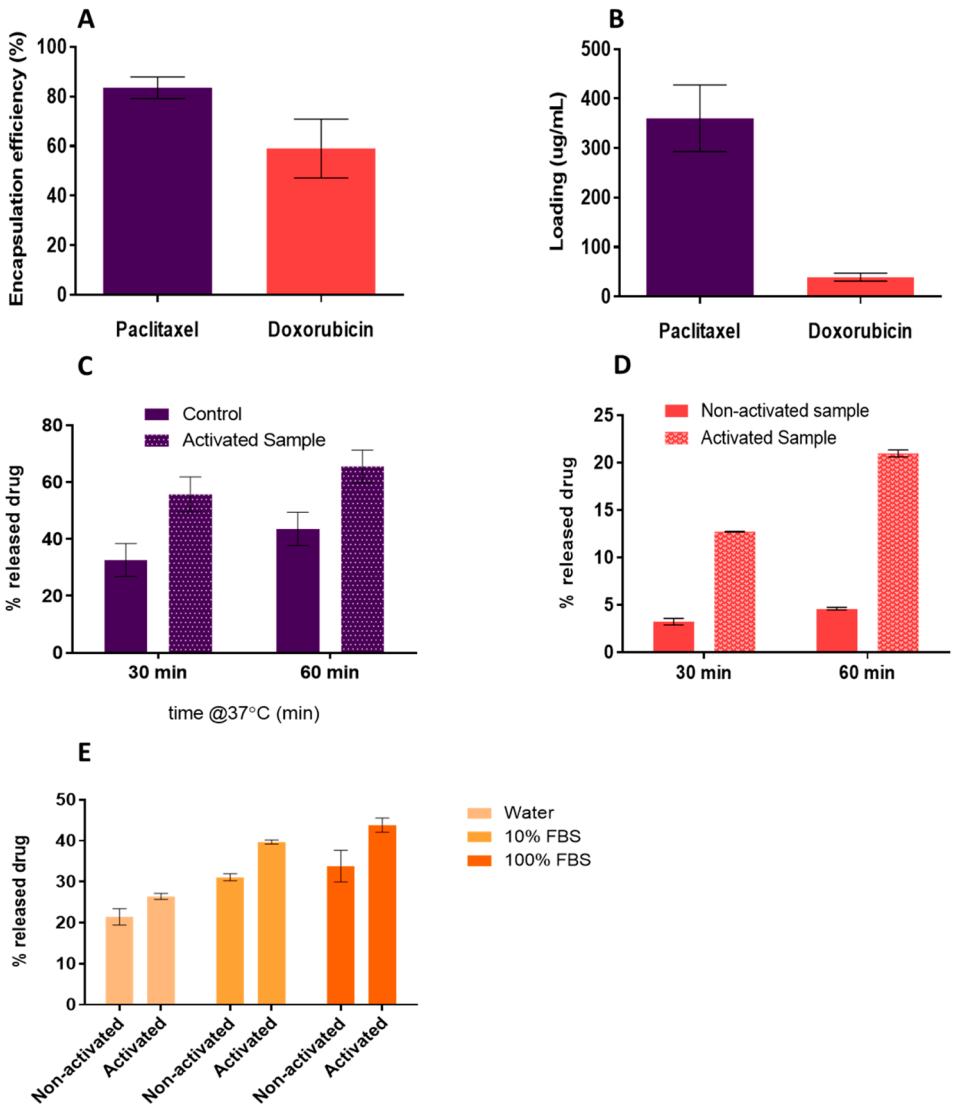

Figure 4. (A) Encapsulation efficiency of paclitaxel and doxorubicin in DDD; (B) loading efficiency for paclitaxel and doxorubicin in double-drug loaded nanodroplets; (C) laser-triggered paclitaxel release from activated DDDs compared to a non-activated control; (D) laser-triggered doxorubicin release from DDD compared to non-activated control; (E) doxorubicin release comparison of nanodroplets preincubated with FBS solutions of various concentrations (0−100% volume). Error bars represent the standard deviation of triplicate experiments.

with DLS measurements taken over the course of 26.5 h. The size trended upward for both samples, most likely due to the coalescence or agglomeration of nanodroplets (Figure 2C). However, the size of nanodroplets after 1 day was still in the submicrometer range indicating a good potential for circulation times and accumulation in leaky tumor tissue.[40] The different media of incubation did not generate a statistically significant difference in the mean size of nanodroplets, due to the rather large variance between measurements. The derived count rate (Figure 2D) shows a large decrease for the BSA-incubated nanodroplets compared to the ones dispersed in water. This could be a result of foam formed during the mixing of the BSA sample, that rises to the top of the dispersion and is not present in the detection window. One thing to note is that the BSA solution itself contributes to the count rate, as micelle or protein agglomerates are detected by the DLS alongside the nanodroplet peaks, as can be seen in the intensity-weighed distribution histograms (Supplementary Figure 2).

Drug Encapsulation and Release. Both paclitaxel and doxorubicin are common chemotherapeutics that are used either as monotherapy or in combination in the treatment of solid tumors. Both drugs have side effects, such as neurotoxicity or cardiotoxicity, that limit their systemic use.[41] Moreover, the two have different solubilities in aqueous media and have distinct mechanisms of cytotoxicity[42] making them good candidates for coencapsulation in the same nanocarrier. Loading both these drugs in nanodroplets bypasses the issue of different pharmacokinetic profiles,[33] ensuring the codelivery at the same time and place.

Figure 3A presents a cross-sectional view of a liquid nanodroplet formed by a double emulsion and loaded with the two drugs. Figure 3B presents the nanodroplets captured with bright field microscopy before activation ("0") and 5 min after sitting on the coverslip without any intervention ("5-"). The next image shows the same droplets immediately after activation with a NIR pulsed laser ("5+"), as well as the progression of the microbubble size after 5 min after activation

https://doi.org/10.1021/acsanm.1c01303
ACS Appl. Nano Mater. XXXX, XXX, XXX−XXX

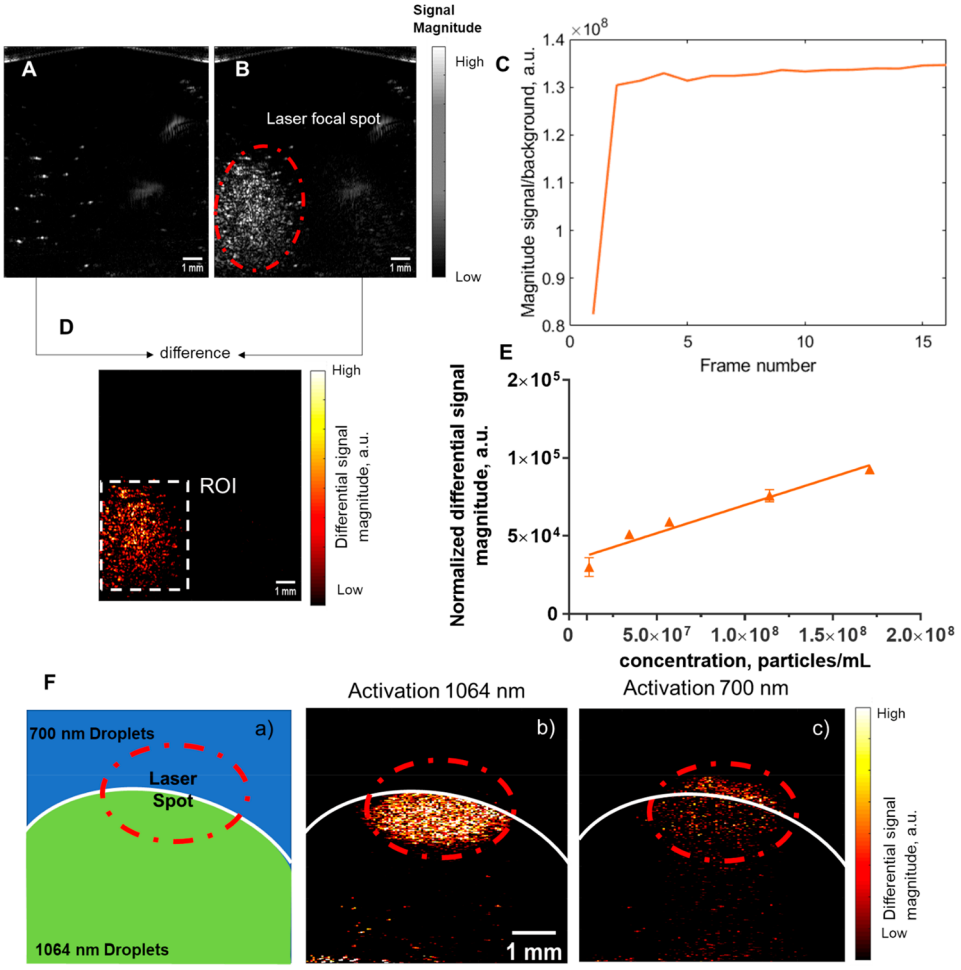

Figure 5. (A) Ultrasound B-scan frame of DDD-laden polyacrylamide phantom prior to activation; (B) ultrasound B-scan frame after 1 laser pulse with visible microbubbles in the laser focal spot (red circle); (C) graph of total intensity in the selected region of interest against frame number, showing a sharp increase of signal at the moment of activation (frame #2); (D) ultrasound difference frame between the frame acquired immediately after activation (#2) and the frame acquired before (#1); (E) graph showing the linear dependency of the differential ultrasound magnitude in the ROI with the concentration of nanodroplets in the phantom. Error bars represent the standard deviation of 4 replicate experiments; (F) schematic (a) and US differential frames of insert phantoms containing neighboring regions encapsulating nanodroplets with different NIR dyes. Activating consecutively by the two corresponding wavelengths shows localized activation of nanodroplets.

("10"). The images showcase the transition of the core from liquid to gas as microbubbles are formed upon exposure of the sample to laser. The microbubbles increase in size after a few minutes, a process that could be explained by the recently described phenomenon of nanodroplets enhancing microbubble inflation in mixtures of the two.[43]

Dual-drug loaded nanodroplets were destroyed in acetonitrile−water 1:1 vol. mixture to dissolve all loaded drugs. Encapsulation efficiencies were measured to be approximately 80% for paclitaxel and 60% for doxorubicin (Figure 4A), corresponding to a loading of 360 ± 67 ug/mL of paclitaxel, and 40 ± 7.9 ug/mL for doxorubicin (Figure 4B). These translate into a loading of 0.36 mg paclitaxel/mg particles and 0.04 mg doxorubicin/mg particles. While this study kept the parameters constant, as to get the same ratio between loaded paclitaxel and loaded doxorubicin, the relatively simple synthesis method allows for this ratio to be modified. This allows for versatility in the effects of the nanodroplets, as different types of cells have been shown to have different optimal ratios for maximum treatment efficacy.[33]

The triggered release of paclitaxel upon nanodroplet vaporization was shown by measuring the release profile with and without external activation for samples kept at 37 °C (Figure 4C). The activated sample was exposed to 5 s of pulsed laser irradiation (with 10 Hz pulse repetition frequency) at the 30 min time point, a small volume was taken out to measure drug release, and the rest of the sample was kept at 37 °C for an additional 30 min, for a total experiment time of 60 min. While the initial samples showed a relatively small amount (~3% with respect the total loaded paclitaxel) of unencapsulated paclitaxel present in the supernatant, after 30 min, both the non-activated and the activated samples had a 10-fold increase in the amount of released paclitaxel. In the case of the non-activated sample, this might be from spontaneous droplet activation, from reorganization of the lipid membrane upon coalescence of droplets, events that are in line with the gradual increase in size and widening of the peak in the size-distribution observed in the DLS measurements. On the other hand, the laser-triggered samples released nearly 50% more paclitaxel than the non-activated control. After an additional 30 min at 37 °C, both samples continued to

https://doi.org/10.1021/acsanm.1c01303
ACS Appl. Nano Mater. XXXX, XXX, XXX−XXX

increase the amount of released paclitaxel in a similar fashion, which is expected due to no additional activation of the samples being performed.

In the case of doxorubicin, a similar experiment was performed, with a batch of nanodroplets being divided into activated and non-activated samples. The "activated" sample was subjected to laser-exposure at the 30 min time point, at which point a small volume of it was removed to measure the released doxorubicin, with the rest of the sample kept at 37 °C for an additional 30 min. To ensure a fair comparison of the activated and non-activated samples, after taking samples for each time point and separating the released doxorubicin in the supernatant, the non-activated samples were subjected to an equivalent laser exposure. This is to correct for photobleaching effects on doxorubicin due to the laser exposure. Figure 4D summarizes the experiment, showing a relatively slow evolution of the released doxorubicin for control droplets, and a jump of over 33% in the amount released from the activated sample immediately after laser activation.

A third experiment related to drug-release was included, investigating the influence of protein corona over the release of drugs (Figure 4E). Doxorubicin was measured in this situation, due to the ease of measurement compared with paclitaxel given its solubility in aqueous media. While passive delivery of drugs has been shown to be impeded by the hard protein corona formed around nanoparticles,[44] we hypothesized that the nanodroplets would be able to overcome the barrier due to the relatively strong mechanical forces generated during activation, that have been shown to be powerful enough to cause cell membrane permeabilization.[45−47] During the experiment, three different conditions of incubation were tested: distilled water, 10% FBS solution, and 100% FBS solution. After a 1 h incubation in their respective media, nanodroplets were resuspended in water and kept for 30 min at 37 °C. The passive and laser-activated doxorubicin releases were measured and compared. The nanodroplets that were kept in water, therefore forming no protein corona, showed results in line with the previous experiment (Figure 4), with some doxorubicin being released passively and a jump in the amount released after laser activation. The effect was more pronounced in the 100% FBS solution. Moreover, laser-activation of the nanodroplets increased the amount of drug release in all cases, with the greatest effect observed in the 100% FBS case. This might be an effect of droplets being closer to one another in dispersion when the protein coronas are larger, allowing for a more efficient transfer of the energy across the droplet population in the sample. This might result in the activation of a higher number of droplets compared to water samples where movement is unencumbered. Additionally, the increased interactions between nanodroplets can cause a broadening of the size of nanodroplets, which relates inversely with the energy needed for activation.[48] Lastly, proteins in the serum might interact with and destabilize the lipid layer of nanodroplets, contributing to the increased passive release of the drug or change the surface charge of the nanodroplets, decreasing the electrostatic interactions between the released doxorubicin and the nanodroplets/microbubbles present in dispersion. Increasing the zeta potential of nanodroplets by using an amine functionalized DSPE-PEG was shown to increase the amount of doxorubicin that is measured in the supernatant after release (Supplementary Figure 3), which supports the hypothesis that surface charge plays an important role in the interaction between nanodroplets and microbubbles and released doxorubicin, impacting the amount of drug that gets detected. This might also explain the disparity between the percentages of released drugs for paclitaxel and doxorubicin.

Ultrasound Imaging. The ultrasound contrast capabilities of nanodroplets before and after activation were investigated in tissue-mimicking polyacrylamide phantoms. A custom ultrasound imaging sequence which consisted of one frame before activation and 15 frames immediately after activation was used. After a single laser pulse, the laser focal spot showed increased contrast compared to the initial liquid droplet state (Figure 5A,B). This is because of the strong acoustic impedance mismatch between the gaseous microbubbles and aqueous background. To obtain the total ultrasound amplitude, a rectangular area surrounding the laser illumination spot was selected as a region of interest (ROI) and the magnitude of pixels in the region was computed as the sum of all pixel values for each frame and denoted the "signal magnitude". Further, the signal magnitude in the ROI was divided by the signal magnitude of the background to calculate the signal-to-background ratio. The results show a strong increase in ultrasound signal-to-background ratio immediately following laser activation of the nanodroplets (Figure 5C). The ratio remains relatively constant for the next 14 frames, indicating that the microbubbles are stable contrast agents for imaging. To obtain the differential signal magnitude, the ultrasound frame immediately preceding the laser activation was subtracted from the ultrasound frame immediately succeeding activation (Figure 5D), and the sum of all pixel values in the same ROI was computed and denoted as the "differential signal magnitude".

To investigate a dependency of the differential signal magnitude in the ROI on the concentration of nanodroplets in the phantom, an experiment was performed using a similar imaging and processing setup as the one described above. The main difference was that the laser exposure time was extended to 5 s to ensure activation of the entire population of nanodroplets. Dual-drug loaded nanodroplets were dispersed in polyacrylamide phantoms with concentrations ranging from 0.1% to 1.5% v/v. This corresponds to a 2×10^7 to 1.5×10^8 particles/mL concentration range, as determined from DLS measurements. The main rationale behind the experiment is to establish that the differential ultrasound signal magnitude is linearly correlated to the number of activated nanodroplets. Thus, the concentration of released drug could be estimated from the images. In the studied range, the phantoms showed a linear dependency of the normalized differential signal (Figure 5E). The normalized differential signal was obtained by computing the differential signal magnitude in the ROI as described before and dividing it by the area of the ROI. With the increase of nanodroplets per unit volume in the focal spot, the normalized differential signal magnitude increases as more microbubbles are created during the activation. The relation between the nanodroplets concentration, and implicitly the concentration of released drugs, and the differential signal is linear in the studied range ($R^2 = 0.9490$). When increasing the concentration of nanodroplets in the phantom above 1.5% v/v, a shadowing effect formed due to the high concentration of microbubbles blocking the signal transmission and reflection. This caused the detected differential signal magnitude in the ROI to drop. Thus, the linearity of the imaging signal is not reliable for very high concentrations of nanodroplets. It is worth noting that in order to find the range of linear response

https://doi.org/10.1021/acsanm.1c01303
ACS Appl. Nano Mater. XXXX, XXX, XXX−XXX

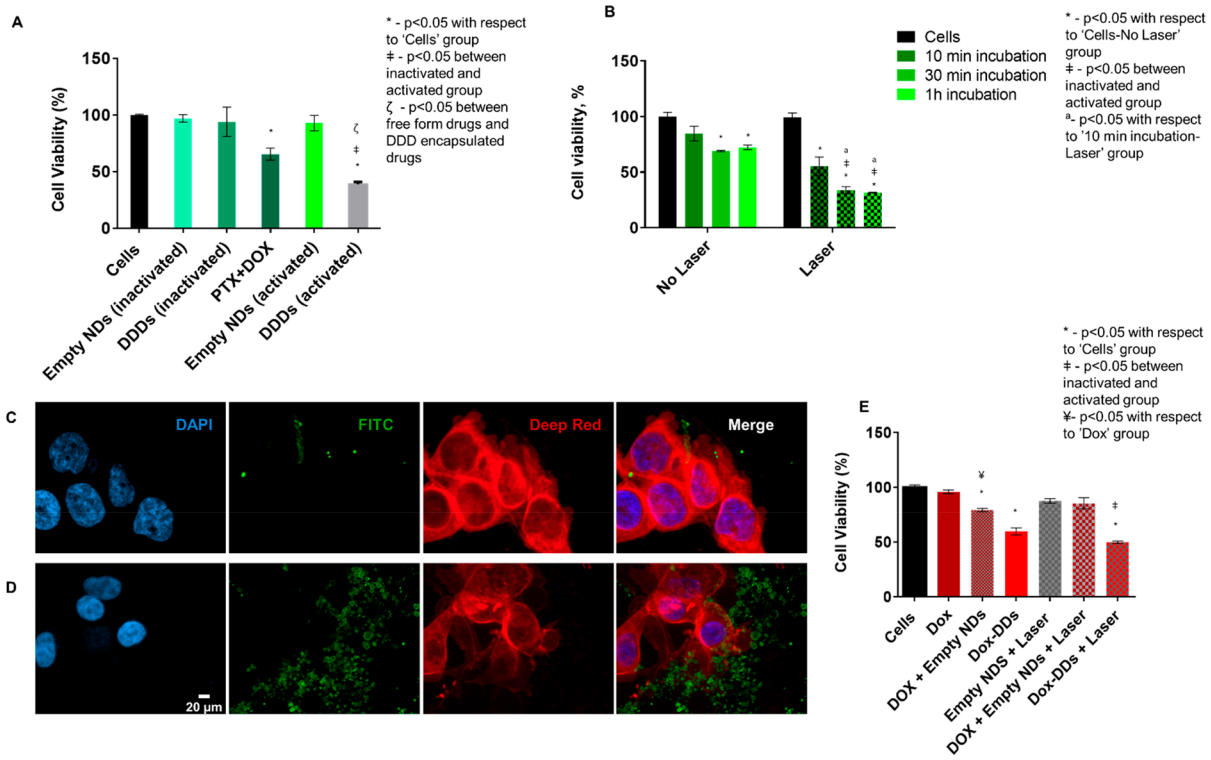

Figure 6. (A) Cytotoxicity of activated nanodroplets compared to control, empty nanodroplets, free drugs (paclitaxel, PTX, and doxorubicin, DOX) and inactivated nanodroplets on FaDu cells. Symbols express the results of student *t* tests between several groups. (B) Comparison of time of activation impact on cytotoxicity. Statistically significant differences between the groups as revealed by Student's *t* test are indicated. (C) Maximum intensity z-projection of confocal fluorescence images of FaDu cells incubated with FITC-labeled nanodroplets (green) for 10 min. Cells were counterstained with DAPI (blue) and CellMask Deep Red (red) for nuclei and plasma membrane, respectively. (D) Maximum intensity z-projection of confocal fluorescence images of FaDu cells incubated with FITC-labeled nanodroplets (green) for 1 h. Cells were counterstained with DAPI (blue) and CellMask Deep Red (red) for nuclei and plasma membrane, respectively. (E) Cytotoxicity of various doxorubicin formulations: free drug, encapsulated in nanodroplets, codelivered with empty nanodroplets to showcase the impact of the activation events on drug internalization. Statistically significant differences are indicated between the groups when relevant. Error bars represent the standard deviation of triplicate experiments.

and obtain a similar accuracy of ultrasound measurement to the one in our study, a calibration process might be involved. This calibration would take into account the nanodroplet characteristics, the ultrasound imaging setup parameters, and the imaging depth. Moreover, as noted in the drug release experiments, the amount of drugs being released by activation is not necessarily 100% of the drugs encapsulated, with other interactions of the nanodroplets and microbubbles matrix and the released drug being a possible factor. Additional work is needed in order to establish the correspondence between the activated nanodroplets and the amount of drugs being released in tissue-mimicking phantoms, which would allow the translation of the ultrasound magnitude to the local concentration of drugs.

One of the advantages of optically activated droplets lies in the possibility to change the dye used for activation, and combine droplets with different dyes for multiplexing.[49] Due to their relatively narrow activation wavelength, we employed two NIR dyes with a peak absorption at 700 nm (Epolight 6698) and 1064 nm (Epolight 3072). Each dye was used for a separate batch of droplets, and an insert polyacrylamide phantom was created, encapsulating the droplets with each of the dyes in neighboring regions (Figure 5F). Consecutive activation with the 1064 nm, and 700 nm at the border of the two regions, shows localized activation of the droplets with the corresponding dye, showcasing the possibility of multiplexing. This could ultimately enable independent timing for the release of distinct cargo.

Overall, what these experiments show is that within a specified range of nanodroplets' concentration, we can use the differential ultrasound magnitude to evaluate the local concentration of activated nanodroplets. In the context of image-guided drug-delivery, this could allow for visualization of the site-accumulation of droplets, and when accounting for the connection between concentration of drug released and the parameters of activation (such as total energy of laser), the effective local drug concentration. In situations where the local concentration of each of the drugs needs to be resolved, multiplex formulations could help disambiguate by individual activation events each with their corresponding differential ultrasound signal. Due to the localized, on demand nature of the activation events, these nanodroplets are a promising and versatile platform for ultrasound-guided drug-delivery.

Nanodroplet Cytotoxicity. Dual drug-loaded droplets were tested for their cytotoxicity on FaDu cells using an MTT assay. FaDu cells are a well-established squamous head and neck cancer in vitro model, and both paclitaxel and doxorubicin are used in therapeutic regimens for this type of disease in combination with one another[50] or other chemotherapeutics.[51] We compared the effect of incubating cells with drug-free nanodroplets against that of paclitaxel and doxorubicin loaded DDDs (Figure 6A). Drug-free nanodroplets,

https://doi.org/10.1021/acsanm.1c01303
ACS Appl. Nano Mater. XXXX, XXX, XXX−XXX

either activated or non-activated, showed no significant cytotoxic effect compared to the control cell group. There was also no significant difference between the activated and non-activated empty droplets, showing that the mechanical effects of the expansion experiences during activation did not considerably affect cell viability. In contrast, activated drug-loaded nanodroplets showed significantly lower cell viability than inactivated drug-loaded nanodroplets ($p = 0.0019$), supporting the hypothesis that NIR activation enables on-demand release of the two drugs. Moreover, compared to cells that were subjected to a combination of free doxorubicin and paclitaxel in the same concentrations as the loaded nanodroplets, the activated DDDs showed significantly greater cytotoxicity ($p = 0.0012$).

We hypothesized that the difference in cytotoxicity between free drugs and nanodroplet-encapsulated drugs stemmed from the release of the drugs in the intracellular space, increasing their efficacy, especially in the case of doxorubicin, which acts by intercalation within DNA strands and inhibition of topoisomerase-II.[52] This would imply that the time between the start of incubation of cells with droplets and their activation would influence their cytotoxicity based on the length of time of the internalization of droplets. To test this hypothesis, the DDDs were activated after either 10 min, 30 min, or 1 h of incubation with FaDu cells. All samples were left for their respective incubation times, media removed, and replaced with fresh media, then subjected to pulsed laser activation, for a total of 10 s at 10 Hz. All groups had a non-activated counterpart to compare to the effect of passive release from inactivated droplets. After 10 min of incubation, the DDDs did not show a significant effect on cells for inactivated droplets but did show a reduction in the cell viability in the case of activated droplets (Figure 6B). All other groups, inactivated and activated, showed statistically significant differences with respect to the cell control. As observed in the previous experiment (Figure 6), all groups showed a significantly greater cytotoxicity when the laser activation stimulus was applied. Moreover, there were significant differences between the activated 10 min group and the activated 30 min or 1 h groups. This is in line with our expectations given the above stated hypothesis.

To further support the hypothesis of time-dependent droplet localization, we studied the internalization of droplets following a 10 min internalization compared to 1 h internalization with confocal fluorescence microscopy. Our results showed a large difference in the number of droplets present in favor of the 1 h incubated sample (Figure 6C−D). Even though the nanodroplets seemed to be mostly bound to the cell membrane for the 1 h incubation time sample, a fraction of them were situated inside the cytosol, in contrast with the 10 min sample where no such examples could be visualized.

Beyond the intracellular localization of nanodroplets at the time of activation compared to extracellular localization in the case of cells incubated for 10 min, mechanical effects of the activation are another factor likely to influence the effect of drugs on cells. Previous studies have shown that cells experience permeabilization of the membrane—and potentially of the nuclear membrane—when exposed to ultrasound waves, such as the ones arising from the acoustical activation of nanodroplets.[45−47,53] To investigate whether the mechanical effects of the activation play a role in the case of our nanodroplets we designed an experiment to compare cells that were incubated with either doxorubicin, doxorubicin and empty nanodroplets, or doxorubicin-loaded nanodroplets (Figure 6E). Doxorubicin was particularly selected as the drug of choice in this situation due to its mechanism of action that involves localization in the cell nucleus,[52] and due to its lower concentration in the nanodroplets that allowed us to increase the number of nanodroplets used in the study without decreasing the population of cells drastically. This test revealed that empty nanodroplets alone did not significantly affect cell viability, while the doxorubicin and empty nanodroplets mixture slightly improved the cytotoxicity of the drug. However, the cells in the drug and activated empty nanodroplets group did not differ significantly from the non-activated equivalent. This indicates that the mechanical effects of the activation are not strong enough to make a difference in this case. In contrast to sonoporation studies,[54] which use minutes-long ultrasound exposure to disrupt cell membranes, the pressure wave produced during the vaporization event only persists on the microsecond time scale. Thus, it is unlikely that drugs external to the cell will be able to experience a strong increase in uptake with this stimulus. Moreover, the activated drug-loaded nanodroplets was the most successful formulation at reducing the cell viability, underlining once more that the spatial colocalization of the nanodroplets and the drug, but also the simultaneous drug release and mechanical effects of activation are needed for an increase in efficacy of the drug.

While the in vitro results for our system are promising, we recognize our technology might present limitations *in vivo*, requiring adjustments to the formulation. One such limitation would be the depth of activation that is achievable by NIR-light, which is on the order of a couple tens of millimeters,[55] with the energy of the penetrating light dropping drastically after that. While in preclinical testing this problem could be avoided, alternative activation mechanisms are possible for applications in which the depth of activation needs to be higher. The vaporization of nanodroplets can be achieved by focused ultrasound, as shown in other studies from our group.[56] Using this technique, depths of several centimeters can be reached. Second, while the size is well in the nanometric domain and a good improvement compared to microbubbles, there are still concerns for systems that rely on passive accumulation, due to heterogeneity of vasculature leakiness.[57] A potential solution to address these concerns could be including active-targeting by surface modifications of nanodroplets,[58,59] or following the activation of nanodroplets with sustained acoustic cavitation to elicit sonoporation effects from the formed microbubbles.[60]

In terms of drugs or active compounds that can be encapsulated in our platform, some limitations that could be related to the structure of the drug are to be expected. In a previous study from our group, a different chemotherapeutic, cisplatin, was used as the drug encapsulated in the core, with results showing that its reduced solubility limited the amount that could be loaded.[61] The choice of hydrophobic compound might also depend on its solubility in chloroform, to enable codissolution with the lipids. Our experience in encapsulating hydrophobic molecules with rather different structures and characteristics, such as paclitaxel, the Epolight dyes showed in the study, as well as other lyphophilic dyes such as DiR and DiD seems promising for the range of compounds that would be suitably loaded onto this type of constructs.

https://doi.org/10.1021/acsanm.1c01303
ACS Appl. Nano Mater. XXXX, XXX, XXX−XXX

4. CONCLUSIONS

In this study, we report the construction and characterization of phase-changing nanodroplets loaded with both paclitaxel and doxorubicin for laser-triggered drug-releasing capabilities. The two chemotherapeutics are concurrently loaded into a core−shell nanodroplet structure, with a perfluoropentane core and a biocompatible lipid shell. Due to the incorporation of a NIR absorbing dye in the shell, the core of the nanodroplet transitions from a liquid to a gaseous phase when exposed to a pulsed NIR laser. This activation results in expulsion of the loaded drugs, and the emergence of microbubbles, which provide high ultrasound contrast. This contrast can be used as a spatially resolved estimation of released drug concentration. In our study, we show that there is a range in which the dependency of the total ultrasound image amplitude and the concentration of activated nanodroplets follows a linear relation. These results contribute toward establishing an ultrasound-based approach to monitoring chemotherapeutics delivered to a specific location.

We characterized the cytotoxicity of the DDDs, noting an enhancement in the effect of triggered nanodroplets compared to free drug formulations. The relatively low effects of non-activated loaded nanodroplets indicate a good stability and control over the drug-release process. The codelivery of two drugs with the same vehicle overcomes the barriers imposed by their different pharmacokinetic profiles, especially given their difference in solubilities.

Overall, our work proposes a nanocarrier design with on-demand drug-release for enhanced efficacy combination therapy that can be monitored by ultrasound imaging. Owing to the accessibility of ultrasound imaging, as well as its good spatial and temporal resolutions, we believe this could be a useful alternative to more complex imaging techniques currently employed.

■ ASSOCIATED CONTENT

Supporting Information

The Supporting Information is available free of charge at https://pubs.acs.org/doi/10.1021/acsanm.1c01303.

Cryo-TEM method description and images showing the morphology of nanodroplets; intensity-weighed size distribution of nanodroplets and table of size average, standard deviation, PDI, and *Y*-intercept from DLS for nanodroplets stability experiments; zeta potential dependent doxorubicin release from nanodroplets (PDF)

■ AUTHOR INFORMATION

Corresponding Author

Geoffrey P. Luke − *Thayer School of Engineering, Dartmouth College, Hanover, New Hampshire 03755, United States; Translational Engineering in Cancer Research Program, Norris Cotton Cancer Center, Lebanon, New Hampshire 03766, United States;* orcid.org/0000-0002-1486-3398; Email: geoffrey.p.luke@dartmouth.edu

Authors

Catalina-Paula Spatarelu − *Thayer School of Engineering, Dartmouth College, Hanover, New Hampshire 03755, United States*

Austin Van Namen − *Thayer School of Engineering, Dartmouth College, Hanover, New Hampshire 03755, United States*

Complete contact information is available at: https://pubs.acs.org/10.1021/acsanm.1c01303

Notes

The authors declare no competing financial interest.

■ ACKNOWLEDGMENTS

This work was funded by a Norris Cotton Cancer Center Pilot Project Grant (G.P.L.) and a Thayer School of Engineering PhD Innovation Fellowship (C-P.S.). The NCI Cancer Center Support Grant 5P30CA023108-37 enabled the TEM analysis. The authors acknowledge support from the Irradiation, Preclinical Imaging and Microscopy Shared Resource in the Norris Cotton Cancer Center at Dartmouth College with NCI Cancer Center Support Grant 5P30 CA023108-41 and NIH S10 SIG award S10OD21616 and bioMT through NIH NIGMS Grant P20-GM113132 for confocal imaging.

■ REFERENCES

(1) Chen, H.; Zhang, W.; Zhu, G.; Xie, J.; Chen, X. Rethinking Cancer Nanotheranostics. *Nat. Rev. Mater.* **2017**, *2* (7), 17024.

(2) Lanza, G. M.; Moonen, C.; Baker, J. R.; Chang, E.; Cheng, Z.; Grodzinski, P.; Ferrara, K.; Hynynen, K.; Kelloff, G.; Lee, Y.-E. K.; Patri, A. K.; Sept, D.; Schnitzer, J. E.; Wood, B. J.; Zhang, M.; Zheng, G.; Farahani, K. Assessing the Barriers to Image-Guided Drug Delivery. *Wiley Interdiscip. Rev.: Nanomed. Nanobiotechnol.* **2014**, *6* (1), 1−14.

(3) Lammers, T.; Kiessling, F.; Hennink, W. E.; Storm, G. Nanotheranostics and Image-Guided Drug Delivery: Current Concepts and Future Directions. *Mol. Pharmaceutics* **2010**, *7* (6), 1899−1912.

(4) Dijkmans, P.; Juffermans, L.; Musters, R.; Vanwamel, a.; Tencate, F.; Vangilst, W.; Visser, C.; Dejong, N.; Kamp, O. Microbubbles and Ultrasound: From Diagnosis to Therapy. *Eur. J. Echocardiogr.* **2004**, *5* (4), 245−256.

(5) Tzu-Yin, W.; Wilson, K. E.; Machtaler, S.; Willmann, J. K. Ultrasound and Microbubble Guided Drug Delivery: Mechanistic Understanding and Clinical Implications. *Curr. Pharm. Biotechnol.* **2014**, *14* (8), 743−752.

(6) Chowdhury, S. M.; Lee, T.; Willmann, J. K. Ultrasound-Guided Drug Delivery in Cancer. *Ultrasonography* **2017**, *36* (3), 171.

(7) Kiessling, F.; Bzyl, J.; Fokong, S.; Siepmann, M.; Schmitz, G.; Palmowski, M. Targeted Ultrasound Imaging of Cancer: An Emerging Technology on Its Way to Clinics. *Curr. Pharm. Des.* **2012**, *18* (15), 2184−2199.

(8) Rapoport, N. Y.; Kennedy, A. M.; Shea, J. E.; Scaife, C. L.; Nam, K.-H. Controlled and Targeted Tumor Chemotherapy by Ultrasound-Activated Nanoemulsions/Microbubbles. *J. Controlled Release* **2009**, *138* (3), 268−276.

(9) Lovelyn, C.; Attama, A. A. Current State of Nanoemulsions in Drug Delivery. *J. Biomater. Nanobiotechnol.* **2011**, *02* (05), 626−639.

(10) Rapoport, N. Phase-Shift, Stimuli-Responsive Perfluorocarbon Nanodroplets for Drug Delivery to Cancer. *Wiley Interdiscip. Rev. Nanomed. Nanobiotechnol.* **2012**, *4* (5), 492−510.

(11) Lanza, G. M.; Winter, P. M.; Caruthers, S. D.; Hughes, M. S.; Hu, G.; Schmieder, A. H.; Wickline, S. A. Theragnostics for Tumor and Plaque Angiogenesis with Perfluorocarbon Nanoemulsions. *Angiogenesis* **2010**, *13* (2), 189−202.

(12) Zhang, M.; Fabiilli, M. L.; Haworth, K. J.; Padilla, F.; Swanson, S. D.; Kripfgans, O. D.; Carson, P. L.; Fowlkes, J. B. Acoustic Droplet Vaporization for Enhancement of Thermal Ablation by High Intensity Focused Ultrasound. *Acad. Radiol.* **2011**, *18* (9), 1123−1132.

(13) Ferenz, K. B.; Steinbicker, A. U. Artificial Oxygen Carriers-Past, Present, and Future-a Review of the Most Innovative and Clinically Relevant Concepts. *J. Pharmacol. Exp. Ther.* **2019**, *369* (2), 300−310.
(14) Jägers, J.; Wrobeln, A.; Ferenz, K. B. Perfluorocarbon-Based Oxygen Carriers: From Physics to Physiology. *Pfluegers Arch.* **2021**, *473* (2), 139−150.
(15) Correas, J. M.; Meuter, A. R.; Singlas, E.; Kessler, D. R.; Worah, D.; Quay, S. C. Human Pharmacokinetics of a Perfluorocarbon Ultrasound Contrast Agent Evaluated with Gas Chromatography. *Ultrasound Med. Biol.* **2001**, *27* (4), 565−570.
(16) Staal, A. H. J.; Becker, K.; Tagit, O.; Koen van Riessen, N.; Koshkina, O.; Veltien, A.; Bouvain, P.; Cortenbach, K. R. G.; Scheenen, T.; Flögel, U.; Temme, S.; Srinivas, M. In Vivo Clearance of 19F MRI Imaging Nanocarriers Is Strongly Influenced by Nanoparticle Ultrastructure. *Biomaterials* **2020**, *261*, 120307.
(17) Jacoby, C.; Temme, S.; Mayenfels, F.; Benoit, N.; Krafft, M. P.; Schubert, R.; Schrader, J.; Flögel, U. Probing Different Perfluorocarbons for in Vivo Inflammation Imaging by ^{19}F MRI: Image Reconstruction, Biological Half-Lives and Sensitivity. *NMR Biomed.* **2014**, *27* (3), 261−271.
(18) Mayer, D.; Ferenz, K. B. Perfluorocarbons for the Treatment of Decompression Illness: How to Bridge the Gap between Theory and Practice. *Eur. J. Appl. Physiol.* **2019**, *119* (11−12), 2421−2433.
(19) Kuznetsova, I. Perfluorocarbon Emulsions: Stability in Vitro and in Vivo (A Review) | Semantic Scholar. *Pharm. Chem. J.* **2003**, *37*, 415.
(20) Kabalnov, A. S.; Makarov, K. N.; Shcherbakova, O. V.; Nesmeyanov, A. N. Solubility of Fluorocarbons in Water as a Key Parameter Determining Fluorocarbon Emulsion Stability. *J. Fluorine Chem.* **1990**, *50* (3), 271−284.
(21) Keipert, P. E.; Otto, S.; Flaim, S. F.; Weers, J. G.; Schutt, E. A.; Pelura, T. J.; Klein, D. H.; Yaksh, T. L. Influence of Perflubron Emulsion Particle Size on Blood Half-Life and Febrile Response in Rats. *Artif. Cells, Blood Substitutes, Biotechnol.* **1994**, *22* (4), 1169−1174.
(22) Sheeran, P. S.; Dayton, P. A. Improving the Performance of Phase-Change Perfluorocarbon Droplets for Medical Ultrasonography: Current Progress, Challenges, and Prospects. *Scientifica* **2014**, *2014*, 1−24.
(23) Sheeran, P. S.; Dayton, P. A. Phase-Change Contrast Agents for Imaging and Therapy. *Curr. Pharm. Des.* **2012**, *18* (15), 2152−2165.
(24) Hallam, K. A.; Donnelly, E. M.; Karpiouk, A. B.; Hartman, R. K.; Emelianov, S. Y. Laser-Activated Perfluorocarbon Nanodroplets: A New Tool for Blood Brain Barrier Opening. *Biomed. Opt. Express* **2018**, *9* (9), 4527.
(25) Lea-Banks, H.; O'Reilly, M. A.; Hynynen, K. Ultrasound-Responsive Droplets for Therapy: A Review. *J. Controlled Release* **2019**, *293*, 144.
(26) Rapoport, N.; Nam, K.; Christensen, D. A.; Kennedy, A. M. Ultrasound-mediated Tumor Chemotherapy with Drug-loaded Phase-shift Nanoemulsions. *J. Acoust. Soc. Am.* **2010**, *127* (3), 1976−1976.
(27) Rapoport, N.; Payne, A.; Dillon, C.; Shea, J.; Scaife, C.; Gupta, R. Focused Ultrasound-Mediated Drug Delivery to Pancreatic Cancer in a Mouse Model. *J. Ther. ultrasound* **2013**, *1*, 11.
(28) Hu, Q.; Sun, W.; Wang, C.; Gu, Z. Recent Advances of Cocktail Chemotherapy by Combination Drug Delivery Systems. *Adv. Drug Delivery Rev.* **2016**, *98*, 19−34.
(29) Jia, J.; Zhu, F.; Ma, X.; Cao, Z. W.; Li, Y. X.; Chen, Y. Z. Mechanisms of Drug Combinations: Interaction and Network Perspectives. *Nat. Rev. Drug Discovery* **2009**, *8* (2), 111−128.
(30) Mokhtari, R. B.; Homayouni, T. S.; Baluch, N.; Morgatskaya, E.; Kumar, S.; Das, B.; Yeger, H. Combination Therapy in Combating Cancer. *Oncotarget* **2017**, *8* (23), 38022−38043.
(31) Mayer, L. D.; Janoff, A. S. Optimizing Combination Chemotherapy by Controlling Drug Ratios. *Mol. Interventions* **2007**, *7* (4), 216−223.
(32) Kratz, F.; Warnecke, A. Finding the Optimal Balance: Challenges of Improving Conventional Cancer Chemotherapy Using Suitable Combinations with Nano-Sized Drug Delivery Systems. *J. Controlled Release* **2012**, *164* (2), 221−235.
(33) Baabur-Cohen, H.; Vossen, L. I.; Krüger, H. R.; Eldar-boock, A.; Yeini, E.; Landa-Rouben, N.; Tiram, G.; Wedepohl, S.; Markovsky, E.; Leor, J.; Calderón, M.; Satchi-Fainaro, R. In Vivo Comparative Study of Distinct Polymeric Architectures Bearing a Combination of Paclitaxel and Doxorubicin at a Synergistic Ratio. *J. Controlled Release* **2017**, *257*, 118−131.
(34) Rapoport, N. *Drug-Loaded Perfluorocarbon Nanodroplets for Ultrasound-Mediated Drug Delivery*; Springer: Cham, 2016; pp 221−241. DOI: 10.1007/978-3-319-22536-4_13.
(35) Hu, C.-M. J.; Zhang, L. Nanoparticle-Based Combination Therapy toward Overcoming Drug Resistance in Cancer. *Biochem. Pharmacol.* **2012**, *83* (8), 1104−1111.
(36) Gianni, L.; Baselga, J.; Eiermann, W.; Porta, V. G.; Semiglazov, V.; Lluch, A.; Zambetti, M.; Sabadell, D.; Raab, G.; Cussac, A. L.; Bozhok, A.; Martinez-Agulló, A.; Greco, M.; Byakhov, M.; Lopez, J. J. L.; Mansutti, M.; Valagussa, P.; Bonadonna, G. Phase III Trial Evaluating the Addition of Paclitaxel to Doxorubicin Followed by Cyclophosphamide, Methotrexate, and Fluorouracil, as Adjuvant or Primary Systemic Therapy: European Cooperative Trial in Operable Breast Cancer. *J. Clin. Oncol.* **2009**, *27* (15), 2474−2481.
(37) Zell, K.; Sperl, J. I.; Vogel, M. W.; Niessner, R.; Haisch, C. Acoustical Properties of Selected Tissue Phantom Materials for Ultrasound Imaging. *Phys. Med. Biol.* **2007**, *52* (20), N475−N484.
(38) *DAPI Counterstaining Protocols*; ThermoFisher Scientific, 2006. https://www.thermofisher.com/us/en/home/references/protocols/cell-and-tissue-analysis/dapi-protocol/basic-dapi-counterstaining-protocols.html
(39) CellMask Deep Red Plasma membrane Stain https://www.thermofisher.com/order/catalog/product/C10046#/C10046 (accessed Feb 24, 2021).
(40) Yoo, J.-W.; Chambers, E.; Mitragotri, S. Factors That Control the Circulation Time of Nanoparticles in Blood: Challenges, Solutions and Future Prospects. *Curr. Pharm. Des.* **2010**, *16* (21), 2298−2307.
(41) Biganzoli, L.; Cufer, T.; Bruning, P.; Coleman, R. E.; Duchateau, L.; Rapoport, B.; Nooij, M.; Delhaye, F.; Miles, D.; Sulkes, A.; Hamilton, A.; Piccart, M. Doxorubicin-Paclitaxel: A Safe Regimen in Terms of Cardiac Toxicity in Metastatic Breast Carcinoma Patients. Results from a European Organization for Research and Treatment of Cancer Multicenter Trial. *Cancer* **2003**, *97* (1), 40−45.
(42) Gustafson, D. L.; Merz, A. L.; Long, M. E. Pharmacokinetics of Combined Doxorubicin and Paclitaxel in Mice. *Cancer Lett.* **2005**, *220* (2), 161−169.
(43) Brambila, C. J.; Lux, J.; Mattrey, R. F.; Boyd, D.; Borden, M. A.; de Gracia Lux, C. Bubble Inflation Using Phase-Change Perfluorocarbon Nanodroplets as a Strategy for Enhanced Ultrasound Imaging and Therapy. *Langmuir* **2020**, *36* (11), 2954−2965.
(44) Behzadi, S.; Serpooshan, V.; Sakhtianchi, R.; Müller, B.; Landfester, K.; Crespy, D.; Mahmoudi, M. Protein Corona Change the Drug Release Profile of Nanocarriers: The "Overlooked" Factor at the Nanobio Interface. *Colloids Surf., B* **2014**, *123*, 143−149.
(45) Liu, W.-W.; Huang, S.-H.; Li, P.-C. Synchronized Optical and Acoustic Droplet Vaporization for Effective Sonoporation. *Pharmaceutics* **2019**, *11* (6), 279.
(46) Zhou, Y.; Yang, K.; Cui, J.; Ye, J. Y.; Deng, C. X. Controlled Permeation of Cell Membrane by Single Bubble Acoustic Cavitation. *J. Controlled Release* **2012**, *157* (1), 103−111.
(47) Qin, D.; Zhang, L.; Chang, N.; Ni, P.; Zong, Y.; Bouakaz, A.; Wan, M.; Feng, Y. In Situ Observation of Single Cell Response to Acoustic Droplet Vaporization: Membrane Deformation, Permeabilization, and Blebbing. *Ultrason. Sonochem.* **2018**, *47*, 141−150.
(48) Wu, Q.; Mannaris, C.; May, J. P.; Bau, L.; Polydorou, A.; Ferri, S.; Carugo, D.; Evans, N. D.; Stride, E. Investigation of the Acoustic Vaporization Threshold of Lipid-Coated Perfluorobutane Nanodroplets Using Both High-Speed Optical Imaging and Acoustic Methods. *Ultrasound Med. Biol.* **2021**, *47*, 1826.

https://doi.org/10.1021/acsanm.1c01303
ACS Appl. Nano Mater. XXXX, XXX, XXX−XXX

(49) Santiesteban, D. Y.; Hallam, K. A.; Yarmoska, S. K.; Emelianov, S. Y. Color-Coded Perfluorocarbon Nanodroplets for Multiplexed Ultrasound and Photoacoustic Imaging. *Nano Res.* **2019**, *12* (4), 741−747.
(50) Airoldi, M.; Cattel, L.; Milla, P.; Pedani, F.; Garzaro, M.; Dosio, F. Paclitaxel and Pegylated Liposomal Doxorubicin in Recurrent Head and Neck Cancer: Clinical and Unexpected Pharmacokinetic Interactions. *Anticancer Res.* **2008**, *28* (4C), 2519.
(51) Bockstein, B.; Vokes, E. Treatment of Metastatic and Recurrent Head and Neck Cancer*UpToDate*; **2021**.
(52) Thorn, C. F.; Oshiro, C.; Marsh, S.; Hernandez-Boussard, T.; McLeod, H.; Klein, T. E.; Altman, R. B. Doxorubicin Pathways: Pharmacodynamics and Adverse Effects. *Pharmacogenet. Genomics* **2011**, *21* (7), 440−446.
(53) Wang, M.; Zhang, Y.; Cai, C.; Tu, J.; Guo, X.; Zhang, D. Sonoporation-Induced Cell Membrane Permeabilization and Cytoskeleton Disassembly at Varied Acoustic and Microbubble-Cell Parameters. *Sci. Rep.* **2018**, *8* (1), 3885.
(54) Liu, W.-W.; Liu, S.-W.; Liou, Y.-R.; Wu, Y.-H.; Yang, Y.-C.; Wang, C.-R. C.; Li, P.-C. Nanodroplet-Vaporization-Assisted Sonoporation for Highly Effective Delivery of Photothermal Treatment. *Sci. Rep.* **2016**, *6* (1), 24753.
(55) Henderson, T. A.; Morries, L. D. Near-Infrared Photonic Energy Penetration: Can Infrared Phototherapy Effectively Reach the Human Brain? *Neuropsychiatr. Dis. Treat.* **2015**, *11*, 2191−2208.
(56) Van Namen, A.; Jandhyala, S.; Jordan, T.; Luke, G. Repeated Acoustic Vaporization of Perfluorohexane Nanodroplets for Contrast-Enhanced Ultrasound Imaging. *IEEE Trans. Ultrason. Ferroelectr. Freq. Control* **2021**, 1.
(57) Danhier, F. To Exploit the Tumor Microenvironment: Since the EPR Effect Fails in the Clinic, What Is the Future of Nanomedicine? *J. Controlled Release* **2016**, *244*, 108−121.
(58) Ishijima, A.; Minamihata, K.; Yamaguchi, S.; Yamahira, S.; Ichikawa, R.; Kobayashi, E.; Iijima, M.; Shibasaki, Y.; Azuma, T.; Nagamune, T.; Sakuma, I. Selective Intracellular Vaporisation of Antibody-Conjugated Phase-Change Nano-Droplets in Vitro. *Sci. Rep.* **2017**, *7* (1), 44077.
(59) de Gracia Lux, C.; Vezeridis, A. M.; Lux, J.; Armstrong, A. M.; Sirsi, S. R.; Hoyt, K.; Mattrey, R. F. Novel Method for the Formation of Monodisperse Superheated Perfluorocarbon Nanodroplets as Activatable Ultrasound Contrast Agents. *RSC Adv.* **2017**, *7* (77), 48561−48568.
(60) Tharkar, P.; Varanasi, R.; Wong, W. S. F.; Jin, C. T.; Chrzanowski, W. Nano-Enhanced Drug Delivery and Therapeutic Ultrasound for Cancer Treatment and Beyond. *Front. Bioeng. Biotechnol.* **2019**, *7*, 324.
(61) Spatarelu, C.-P.; Jandhyala, S.; Luke, G. P. Dual-Drug Loaded Phase-Changing Nanodroplets for Image-Guided Tumor Therapy. In *Colloidal Nanoparticles for Biomedical Applications XV*; Osiński, M., Kanaras, A. G., Eds.; SPIE, 2020; Vol. *11255*, p 31. DOI: 10.1117/12.2542339.

https://doi.org/10.1021/acsanm.1c01303
ACS Appl. Nano Mater. XXXX, XXX, XXX−XXX